A VISUAL EXPERIMENT OF BUBBLE GROWTH PROCESSES IN VERTICAL RECTANGULAR CHANNELS WITH DIFFERENT FLOW PATH HEIGHTS

Ning CHENG[1], Yun GUO[1], Changhong PENG [1], Yong ZHANG[2, 3]
1. School of Nuclear Science and Technology, University of Science and Technology of China, Hefei, Anhui, 230026, China
2. Science and Technology on Reactor System Design Technology Laboratory, Nuclear Power Institute of China, Chengdu 610213, China;
3. Nuclear Power Institute of China, Chengdu, 610213, China;
Corresponding author: Changhong PENG, e-mail: pengch@ustc.edu.cn

REFERENCE NO

NUCL-01

Keywords:
Visual experiment; Bubble growth; micro channel; macro channel; Confinement effects;

ABSTRACT

Bubble growth processes under subcooled flow boiling condition in vertical rectangular channels with gaps of 1.8 mm and 2.8 mm were visually and numerically investigated. Deionized water was used as working fluid and the bubble growth processes were recorded by a high speed camera at a rate of 6000 fps. It has been observed that the channel confinement effects in 1.8mm-gap channel made the bubble behaviours different from those in 2.8mm-gap channel. Bubbles in 1.8mm-gap channel were smaller in size and would fluctuate during growth process, while bubbles in 2.8mm-gap channel could lift off from the heating wall and condense in the subcooled mainstream more easily. The growth curves of bubbles generated under different heating powers, inlet fluid temperatures and mass flow rates were compared and found that within the experimental range the changes of heating power and inlet fluid temperature had a significant effect on bubble growth in both channels.

1. INTRODUCTION

Flow boiling in micro channel has been a hot research topic in recent years due to its effective heat transfer capability. Bubble growth is a basic problem in flow boiling and many researches about bubble growth have been done in previous works but few of them were conducted in narrow rectangular channel which may be used in research reactor and engineering test reactor. The bubble growth processes in narrow rectangular channel will be more complicated than those in traditional large-size circular pipe due to the differences in cross-section shape and channel size. In this work, the bubble growth processes in rectangular channels with gaps of 1.8mm and 2.8mm were visually and numerically investigated, some differences in bubble behaviours were observed and the growth curves of bubbles generated under different conditions were also obtained.

There are many definitions of micro channel in previous work: Kandlikar [1] proposed that the hydraulic diameter D_h of small size channel should be smaller than 3 mm. Mehendale et. al. [2] considered that the distinction between macro- and micro-scale channel is somewhere between 1mm and 6mm in terms of hydraulic diameter. Kew and Cornwell [3] proposed that the channel confinement effects would be significant when the value of confinement number Co was in excess of 0.5 and Co was defined as:

$$\mathrm{Co} = \sqrt{\sigma / g(\rho_l - \rho_v) D_h^2} \qquad (1)$$

In this experiment, the Co numbers are 0.70 and 0.46 for 1.8mm-gap channel and 2.8mm-gap channel respectively, so the 1.8mm-gap channel can be defined as micro channel while the 2.8mm-gap channel is macro channel

2. EXPERIMENTAL CIRCUIT

The experimental circuit is shown in Fig.1 where the pressurizer and vent valve can control system pressure; the shield pump provides a pressure difference for the circuit; three groups of parallel butterfly valves and three flow meters（$\leqslant \pm$ 0.3 kg/h）are used for flow rate adjustments; the preheater can heat the fluid to a specified temperature; the heat exchanger can transfer excess heat from the primary circuit to the secondary circuit.

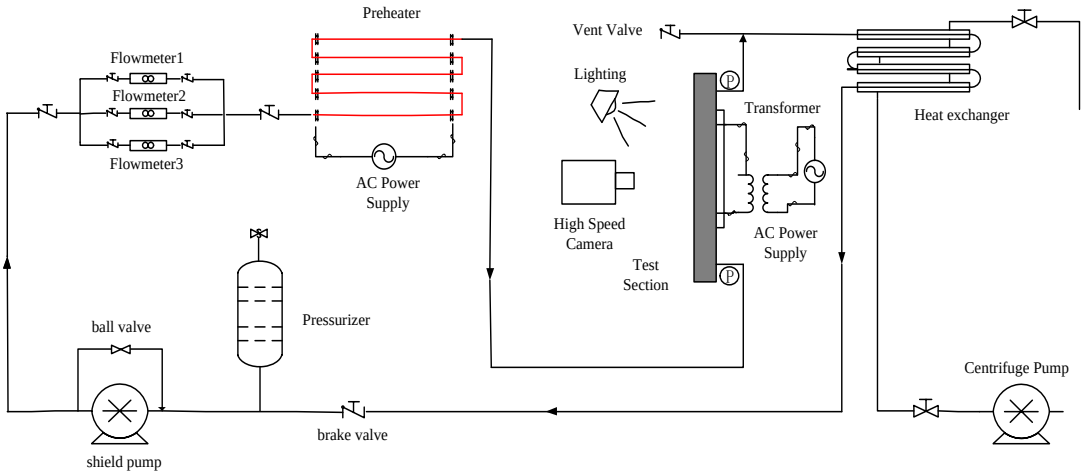

Fig. 1. Experimental circuit

Before the experiment began, the deionized water should be repeatedly heated until the gas dissolved in water was totally removed. During the experiment, the degassed deionized water flowed at a constant mass flow rate and it would be heated to a specified temperature by the preheater before flowing into the test section. Then the water was heated to boiling in the test section and the heating power was controlled by a transformer. A high speed camera of PHANTOM was installed upon the test section to observe and record bubble behaviours at a rate of 6000 frames per second. The photo resolution was 768 pixel × 768 pixel and the scale of corresponding shooting area was 10mm×10mm approximately. The measurement uncertainty of photograph was about one pixel (13μm) for there were shadows around the bubble caused by lighting. Pressure sensors (± 250 Pa) and K-type thermocouples (± 0.2°C) were located at the inlet and outlet of the test section to measure pressure and fluid temperature. The pressure of test section was kept at about one standard atmosphere by pressurizer and vent valve during the experiment.

The schematic diagram and cross-section of test section are shown in Fig.2 (a) and Fig.2 (b). It can be seen in Fig.2 (a) that the test section mainly consists of pressing plate, high temperature resistance glass, stain less steel plate and heating plate. The scales of two flow runners are 610.0 mm × 60.0 mm × 1.8 mm and 610.0 mm × 60.0 mm ×2.8 mm and hydraulic diameters are 3.5 mm and 5.4 mm respectively. There are thin rubber blankets between the glass and the steel plate to avoid leaking and disperse pressure. Ten grooves are uniformly distributed on the back of the steel plate for placing 1 mm-diameter K-type thermocouples (± 0.2°C) to measure the temperature. And heat-dissipating silicon grease is coated on the back of the steel plate to make the heat flow even.

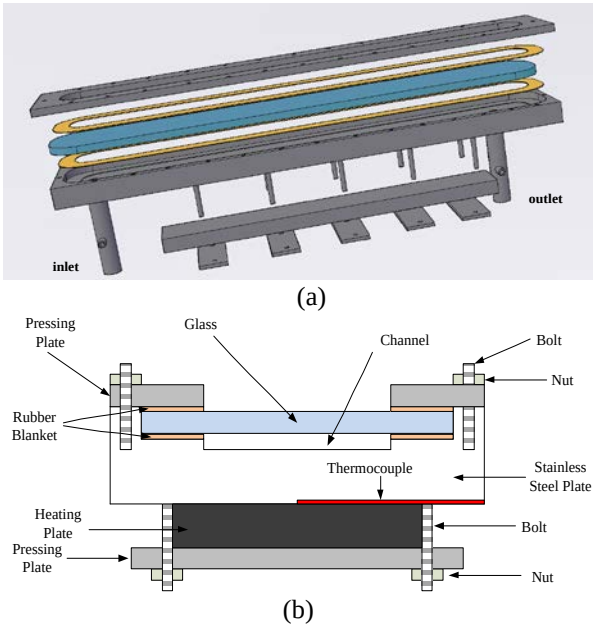

Fig. 2. The schematic diagram (a) and cross-section (b) of the test section

3. EXPERIMENTAL RESULTS AND ANALYSIS

3.1. Data processing

In the experiment, the mass flow rate changed from about 18.4 kg/h to 55.1 kg/h in 1.8 mm-gap channel and from about 20 kg/h to

60 kg/h in 2.8 mm-gap channel, corresponding *Re* ranged from about 500 to 1500. So the experiment was conducted under laminar flow condition. The inlet fluid temperature ranged from 65°C to 90°C and the heating power was between 0.1kW and 1.1 kW.

Suppose the bubble is ellipsoid during the growth process. Since the images are taken from the front direction, only the length of the major axis *a* and the minor axis *b* of the bubble can be obtained. The length of the minor axis *c* in the normal direction of the wall can't be measured directly. The length of *c* couldn't be larger than *a* for the bubble growth will be limited by the height of the channel in micro channel. So assume $c = b$ [4], the equivalent radius can be calculated by Eq. (2) based on the equal volume principle. For consistency, the equivalent bubble radiuses in both pipes will be got in this way in the following passage.

$$R = （\mathrm{abc}）^{1/3}/2 \tag{2}$$

Bubble growth is a complex phenomenon. It is generally accepted that the initial stage of bubble growth is a transient inertial control stage, then is the thermal diffusion control stage. Experiments in traditional large-scale channel show that the variations of equivalent bubble radiuses during thermal diffusion stage can be fitted by Eq. (3) [5] where *R* is equivalent bubble radius, *k* and *n* are empirical parameters. The form of Eq. (3) will also be used to fit bubble growth trends in the following article.

$$R = k \cdot t^n \tag{3}$$

Some of the experimental conditions and data processing results are listed in Table 1, where the letters in Exp. No. indicate the operating conditions; the number 1 stands for the 1.8 mm-gap channel and the number 2 indicates the 2.8 mm-gap channel; *M* stands for the mass flow rate; T_{in} is the inlet fluid temperature; *P* is the heating power; η is the heating efficiency obtained by the single-phase experiment under the same flow and heating conditions; T_a indicates the average fluid temperature at the height of nucleation point. The back of the steel plate is heated by a uniform heat flow, so it can be supposed that the average fluid temperature changes linearly in the heating section and T_a can be written as:

$$T_a = T_{in} + \frac{P\eta L_n}{Mc_pL_t} \tag{4}$$

Where c_p represents the specific heat capacity of water; L_n is the distance from the nucleation point to the start point of heating section and L_t is the total length of heating section.

3.2. Comparison of bubbles in two channels

3.2.1. Confined bubble growth

Fig.3 (a) shows the forces acting on a bubble in vertical micro channel, where the left wall represents glass, the right wall stands for heating wall and the arrows indicate the flow direction. The following equations can be obtained according to reference [6], based on the conservation of momentum.

$$\Sigma F_x = F_{sx} + F_{grx} + F_{sl} + F_{cp} = F_{rx} \tag{5}$$

$$\Sigma F_y = F_{sy} + F_{gry} + F_{bulk} + F_{qs} + F_b = F_{ry} \tag{6}$$

where F_s is the surface tension force; F_{gr}, the bubble growth force caused by the pressure distribution surrounding a growing bubble; F_{sl}, the shear lift force; F_{cp}, the contact pressure force accounting for the bubble being in contact with a solid rather than being surrounded by liquid; F_{bulk}, an additional added-mass force due to the steady liquid flow around the growing bubble; F_{qs}, the quasi steady drag force in the flow direction; F_b, the buoyancy force and F_r; the reaction force acting on the bubble through the three-phase line to balance those other forces acting on the bubble before bubble detachment [7]. ΣF_x and ΣF_y will be balance by F_{rx} and F_{ry}, when the force balance in Y direction is broken and the force balance in X direction is still met, bubble will departure from the nucleation site. If the forces balance in X direction is broken instead of that in Y direction, the bubble will lift-off from the heating wall. In flow boiling, if the bubble lift off from the wall, it will definitely depart from the nucleation site, for F_{ry} is equal to 0 and the

force balance in Y direction must be broken when the bubble doesn't contact the wall.
The forces acting in X direction can be calculated by following equations according to references [7], [8] and [9].

$$F_{sx} \approx -d_w \sigma \frac{\pi}{\theta_a - \theta_r}(cos\theta_r - cos\theta_a) \quad (7)$$

$$F_{grx} = -\rho_l \pi d_w^2 (\frac{3}{2} C_s \dot{R}^2 + R\ddot{R}) cos\theta_c \quad (8)$$

$$F_{sl} = \frac{1}{2} C_{L1} \frac{0.5 d_w}{R} A \rho_l U_c e_x + C_{L2} \rho_l V_b |U_c \times w| e_x \quad (9)$$

$$F_{cp} = \frac{1}{2} d_w^2 \frac{\sigma}{r_c} \quad (10)$$

Where d_w indicates bubble contact circle diameter; σ is surface tension coefficient; θ_a, θ_r, θ_c indicate advancing contact angle, receding contact angle and bubble inclining angle respectively; C_s, C_{L1} and C_{L2} are empirical constants; A is the bubble cross section area perpendicular to the flow; U_c is the velocity of the supposed streamline through the mass centre of the bubble V_b is the bubble volume; ω is the vorticity; e_x is the unit vector in X direction; r_c is the radius of curvature at the reference point. It can be seen from the expressions and definitions of these forces that only F_{gr} can reflect the effects of channel size by adjusting empirical constant C_s and in macro-scale pool boiling C_s = 20/3 is recommended. But it is unsuitable for micro channel. In term of micro channel, the growing bubble can't push away surrounding water freely in the bubble height direction and lead to a significant increase in bubble growth force which will influence bubble behaviours.

It can be observed in the experiment that many bubbles in 2.8mm-gap channel can lift to subcooled mainstream and shrink while most of the bubbles in 1.8mm-gap channel can hardly depart from the nucleation sites under similar flow and heating conditions. So it can be concluded that the bubbles in 2.8mm-gap channel can lift off more easily than those in 1.8 mm-gap channel for the increase of F_{gr} in X direction hinders the bubble from lifting off.

It has been observed by high speed camera that some bubbles in 1.8mm-gap channel will change size periodically during growth process. This may be caused by both phase change and confinement effects. It should be noted that the bubble confined effects mentioned in this article indicates the bubble growth is confined by channel size when the bubble doesn't occupy the whole micro-channel cross-section. Fig.3 (b) shows the phase change process on the bubble in subcooled boiling flow. Evaporation occurs in superheated layer and bubble base while condensation occurs on the top of bubble cap at the same time. The evaporation and condensation occur in both channels under similar flow and heating conditions while the fluctuation of bubble size can only be observed in some cases in 1.8mm-gap channel just like what has been observed in reference [10]. So the channel confinement effects must play an important role in the process. Fig.3 (c) presents the variation of bubble contour in vertical micro channel. The solid bubble profile represents stage I and the dashed one represents stage II. The bubble shape is close to a truncated sphere in stage I and a flat ellipsoid in stage II. The bubble contour will change between stage I and stage II periodically during the growth process and the bubble radius got by images will have small fluctuations for the photographs are taken from the front direction. In stage I, the bubble is still growing with a relative small bubble growth force. When the bubble height is large enough comparing to the height of channel, the bubble growth force increased significantly. This force along the normal direction of the wall and press the bubble on the heating surface. Thus it will prevent the bubble from growing up in this direction then the bubble expands along the channel axial direction, and the bubble shape transforms from a truncated sphere to a flat ellipsoid just like stage II. After the deformation, condensation is greatly enhanced for more bubble cap is exposed to subcooled mainstream. Thus the bubble size decreases and the bubble shape changes back to truncated sphere for the effects of surface tension force. It's hard for evaporation, condensation and forces in X direction to find a completely balanced state due to the flow instability. Therefore the bubble shape will change between stage I and stage II periodically. This character of confined bubble can also be

reflected by the periodic variation of the maximum local void fraction $\alpha$and the bubble aspect ratio β according to [11], α and β can be defined as:

$$\alpha = \frac{c}{H} \quad (11)$$

$$\beta = \frac{c}{a} \quad (12)$$

H in Eq. (11) is the channel height.

3.2.2. Bubble growth in macro scale channel

Fig. 4 presents a bubble growth process in vertical macro channel with no obvious channel confinement effects. In the figures, the left wall represents glass and the right wall stands for heating wall. Each picture represents a stage of bubble growth: the bubble generate at nucleation site (a); volume increase for evaporation (b); depart from the nucleation site and slide along the wall (c). Sometimes the bubble can lift off from the wall (d), condense and shrink (e) in the subcooled main fluid. This kind of bubble can be observed in both channels.

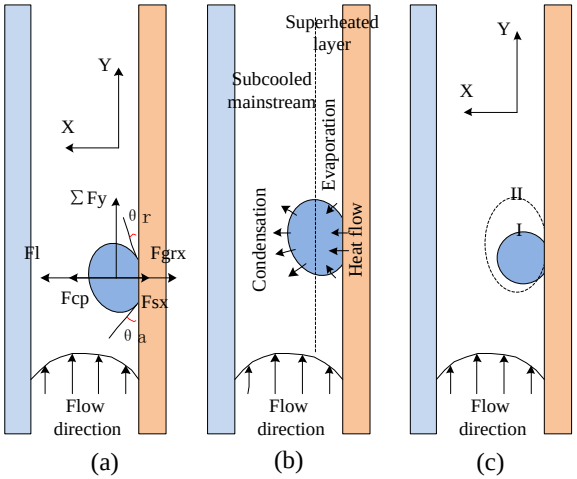

Fig. 3. The schematic diagram of a bubble in vertical micro channel: (a) force analysis; (b) evaporation and condensation; (c) variations of bubble contour

Table 1. Some of the experimental conditions and data processing results

Exp. No.	M (kg/h)	T_{in} (°C)	P (W)	η	T_m (°C)	Re	k	n
A1	36.9	80.2	445	0.81	84.5	912	0.054	0.184
B1	36.9	80.3	505	0.84	85.3	912	0.053	0.254
C1	36.9	80.3	551	0.84	85.8	912	0.078	0.281
C2	39.9	81.0	551	0.83	86.0	967	0.133	0.248
D1	46.1	83.6	400	0.90	87.0	1139	0.043	0.174
D2	50.1	84.2	400	0.87	87.2	1214	0.112	0.319
E1	46.1	83.8	505	0.91	88.2	1139	0.092	0.277
F1	46.2	85.6	363	0.89	88.7	1142	0.048	0.216
F2	49.8	87.8	363	0.89	90.6	1206	0.105	0.301
G1	46.2	85.6	400	0.90	89.0	1142	0.070	0.341
H1	46.3	89.4	300	0.70	91.4	1144	0.073	0.280
I1	55.1	76.2	692	0.91	81.2	1362	0.062	0.169
I2	59.7	75.0	692	0.93	79.6	1447	0.099	0.252
J1	55.3	81.3	505	0.84	84.6	1367	0.056	0.172
J2	60.3	80.3	505	0.90	83.5	1461	0.087	0.281
K1	55.2	87.8	619	0.82	91.8	1364	0.125	0.242
L2	20.0	85.6	400	0.61	90.8	482	0.243	0.239
M2	30.2	87.4	400	0.74	91.7	733	0.110	0.321
N2	49.8	75.8	619	0.92	80.7	1207	0.101	0.298
O2	49.7	75.9	692	0.92	81.4	1204	0.088	0.295
P2	50.1	71.4	794	0.92	77.7	1214	0.060	0.433
Q2	60.2	71.8	692	0.93	76.4	1459	0.068	0.141
R2	59.8	68.2	794	0.93	73.6	1449	0.086	0.227
S2	60.1	68.4	905	0.93	74.6	1457	0.072	0.358
T2	60.3	84.0	505	0.90	87.2	1461	0.095	0.377

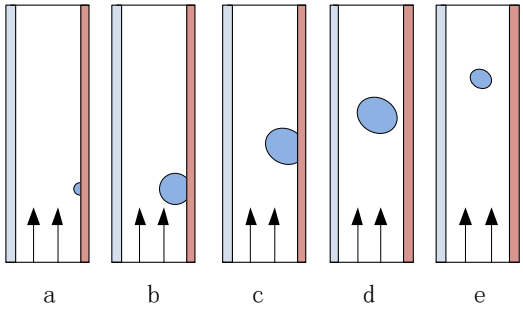

Fig. 4. A bubble growth process in vertical macro channel

Fig.5 (a) corresponds to (a)-(c) stages in Fig.4 under C2 condition and Fig.5 (b) corresponds to (a)-(e) stages in Fig.4 under L2 condition. Fig.6 presents the bubble growth curves fitted by Eq. (3). It can be found that the bubbles are not significantly affected by confinement effects and growth curves strictly follow the Eq. (3) at least before bubbles leaving the nucleation site.

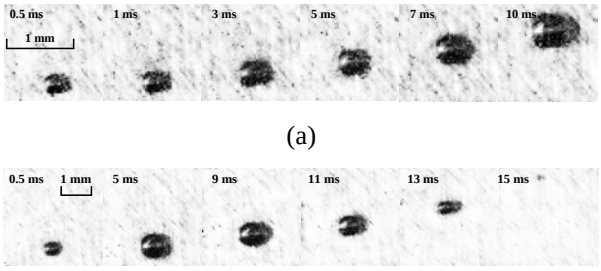

Fig. 5. Photographs of sample bubbles in case C2 (a) and case L2 (b).

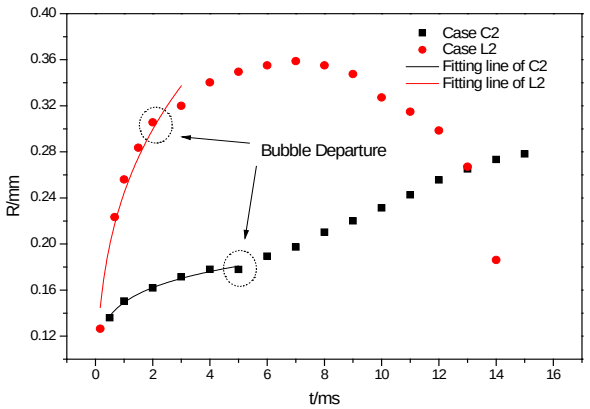

Fig. 6. Variations of equivalent bubble radius in case C2 and case L2

3.2.3. Bubble growth in micro scale channel

Fig.7 shows a bubble growth process in vertical micro channel with significant channel confinement effects. Six pictures represent six stages during the process respectively: the bubble generate at nucleation site (a); volume increase for evaporation (b); deform due to the confinement effects (c); shape recovery (d). Some bubbles can hardly depart from the nucleation point and repeat stage (c) and stage (d). But some bubbles can depart from the nucleation point and slide along the wall (e) affected by flow, buoyancy and surrounding bubbles. This phenomenon can only be observed in 1.8mm-gap channel in the experiment.

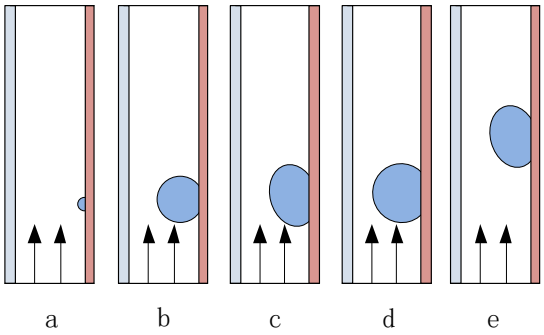

Fig. 7. A bubble growth process in vertical micro channel

Fig.8 (a) corresponds to (a)-(d) stages in Fig.7 under K1 condition and Fig.8 (b) corresponds (a)-(e) stages in Fig.7 under I1 condition. Fig.9 presents the bubble growth curves fitted by Eq. (3). It can be found that the bubble growth trends can be well fitted by Eq. (3) before the occurrence of confinement effects.

This phenomenon is not exactly the same as what has been observed by Liaofei Yin and Li Jia [11]. The bubble has not been elongated and the bubble growth rate doesn't increased after channel confinement effects occur. Because in this experiment the observed bubble is in subcooled fluid and the temperature of mainstream is much lower that saturation temperature. The condensation phenomenon at the cap top will prevent the bubble from growing up and it can counteract the strengthened evaporation effects at bubble root. What's more, the size of channel height in this experiment is much larger than that in the literature, which means the channel confinement effects are much weaker. So the elongated bubble and the increase of bubble growth rate have not been observed.

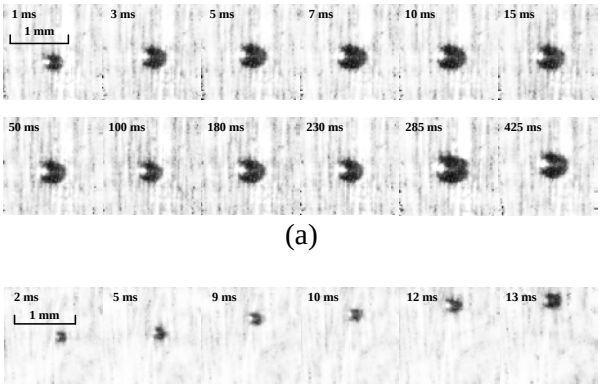

Fig. 8. Images of sample bubbles in case K1 (a) and case I1 (b)

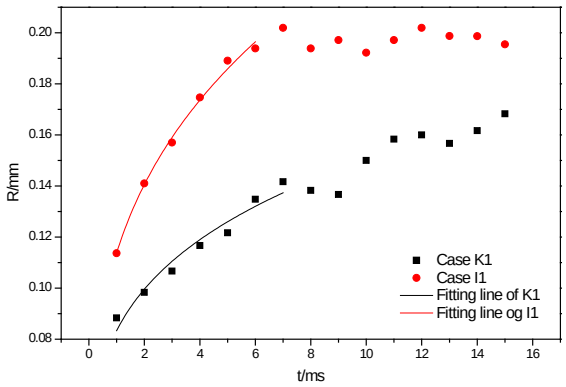

Fig. 9. Equivalent bubble radius variations in case K1 and case I1.

3.2.4. Numerical Simulation

The bubble growth processes in Fig. 5 (b) and Fig.8 (a) have been numerically studied to understand the bubble behaviours better. The volume of fluid method (VOF) in commercial software ANSYS FLUENT was used to simulate the bubble growth processes under two dimensional condition. Fig.10 and Fig.11 present the computational results from the side direction, where red colour represents vapour phase and blue colour represents liquid phase. In each case, the computational region is a small part of the whole channel and the width of each picture is equal to the height of channel. To get the inlet fluid temperature and velocity distribution of computational region, a steady state of single phase flow in the whole channel was calculated at first and the distributions of temperature and velocity at the height of nucleation site were extracted as inlet fluid conditions for computational region. It can be found in Fig.10 and Fig.11 that the bubble growth processes in case L2 and case K1 have some differences： In case K1, the bubble stays at the nucleation site and constantly changes shape during growth process, while in case L2 the bubble lifts off from the heating wall and shrinks in the subcooled mainstream. Fig.12 shows the comparison of equivalent bubble radiuses got by experiment and simulation. It can be concluded that the numerical simulation can get the same results as experiment but some errors still exist.

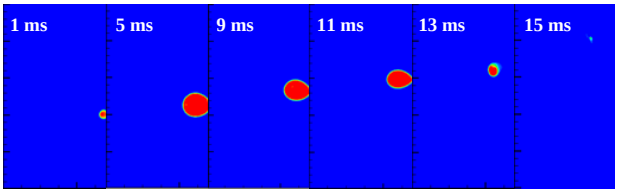

Fig. 10. Bubble growth process of case L2 got by numerical simulation

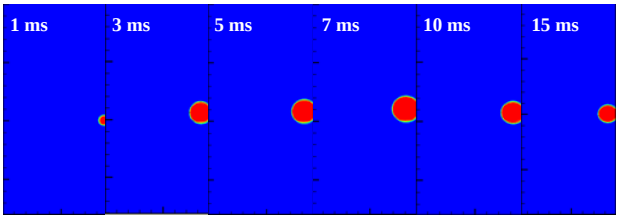

Fig. 11. Bubble growth process of case K1 got by numerical simulation

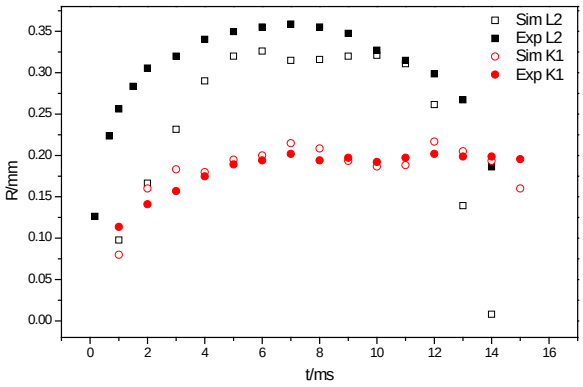

Fig. 12. Comparison of equivalent bubble radiuses got by experiment and simulation in case L2 and case K1.

3.2.5. Comparison of bubble size

Five groups of cases listed in Table1 are presented in Fig.13. There are two sets of experimental data in each group, one is got in 1.8mm-gap channel and is indicated by hollow symbols in the figure; the other is got in 2.8mm-gap channel and is indicated by solid symbols with the same colour. Cases in the

same group have the same heating power, very close inlet fluid temperature and Reynolds number. Obviously, the bubbles generated in 1.8mm-gap channel are smaller in size with smaller value of *k* according to Table 1 than those in 2.8mm-gap channel. So it can be concluded that the bubbles generated in 1.8 mm-gap rectangular channel are smaller than those in 2.8 mm-gap rectangular channel under similar heating and flow conditions in this experiment.

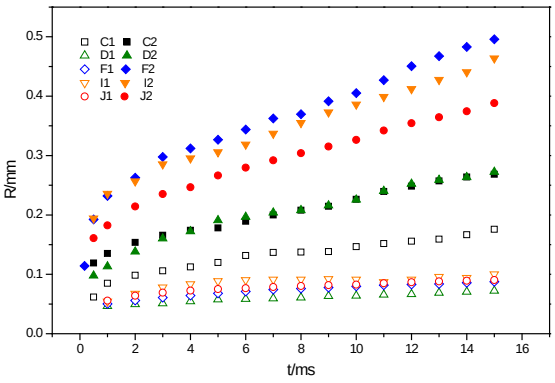

Fig. 13. Comparison of bubble sizes in two channels under similar heating and flow conditions

3.3. Comparison of bubbles under different work conditions

3.3.1. Heating power

Fig.14 shows the comparison of average equivalent bubble radiuses in 1.8mm-gap channel with different heating powers. The first group of data includes cases A1, B1 and C1 and the second group contains cases F1, G1 and E1. One colour represents one group of data and in each group the mass flow rate and mainstream temperature have little differences, while the heating power constantly increases. It can be found that the bubble size increases with heating power in 1.8mm-gap channel. Similar comparison of bubbles in 2.8mm-gap is shown in Fig.15, the bubble size increases with heating power in the first group which contains cases Q2, R2 and S2 while it decreases with increasing heating power in the second group which contains case N2 and case O2. So the change of heating power can influence the bubble growth, but there is no obvious law within the experimental range. Because on the one hand increase heating power can enhance the absorption of energy from the wall and promote the evaporation. On the other hand, the growth of bubble disturbs the overheat boundary layer and adversely affects bubble growth.

3.3.2. Inlet fluid temperature

Two groups of experiments are taken as examples to investigate the influence of inlet fluid temperature with mass flow rate and heating power keep unchanged. Fig.16 and Fig.17 present the comparisons of average equivalent bubble radiuses in 1.8mm-gap channel and 2.8mm-gap channel respectively. Apparently, in both channels, the bubble is larger and grows faster when inlet fluid temperature is higher, corresponding to lager values of *k* and *n* in Tab.1. Because the higher inlet temperature leads to the higher average fluid temperature and the higher superheated boundary layer temperature at the nucleation point and they are beneficial to evaporation.

3.3.3. Mass flow rate

The heating power and inlet fluid temperature remain unchanged to study the influence of the mass flow rate on the bubble. Average equivalent bubble radiuses in B1, J1 ; M2, D2 and I2, O2 are shown in Fig.18. It can be seen that the change of mass flow has little influence on bubble growth in both channels within the experimental rage. This may due to the change of mass flow rate is too small to have an obvious effect in experimental range.

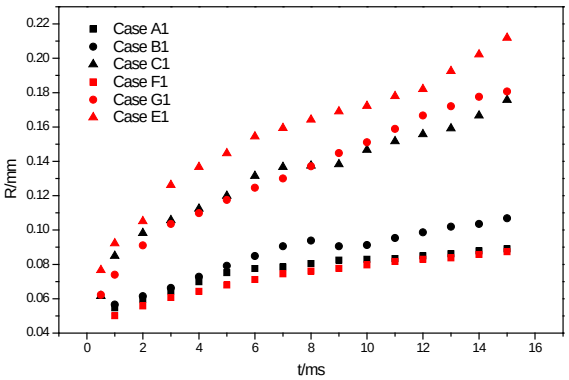

Fig. 14. Comparison of average equivalent bubble radiuses in 1.8mm-gap channel with different heating powers

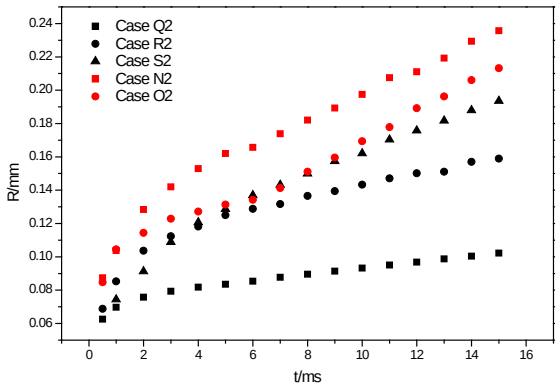

Fig. 15. Comparison of average equivalent bubble radiuses in 2.8mm-gap channel with different heating powers

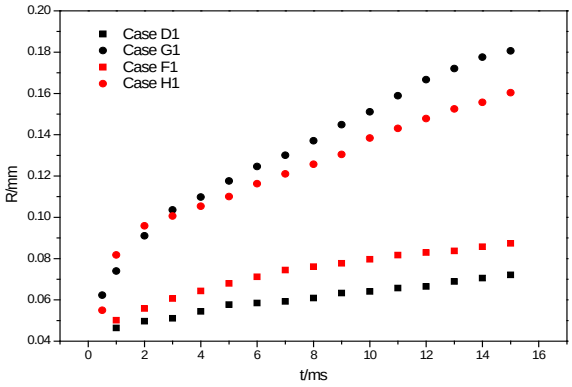

Fig. 16. Comparison of average equivalent bubble radiuses in 1.8mm-gap channel with different inlet fluid temperatures

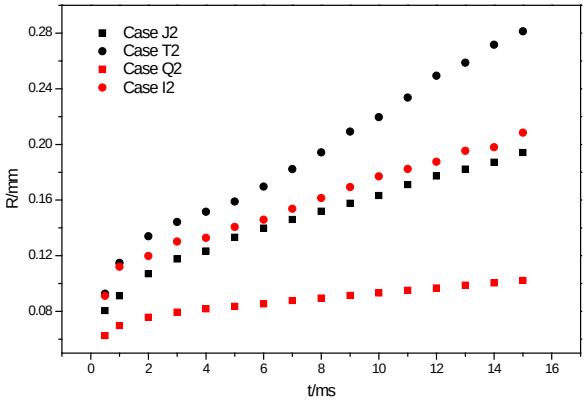

Fig. 17. Comparison of average equivalent bubble radiuses in 2.8mm-gap channel with different inlet fluid temperatures

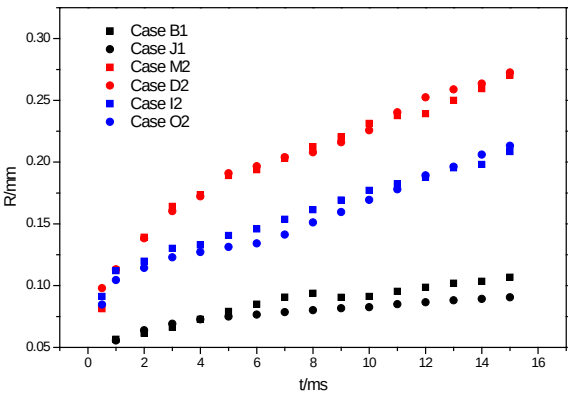

Fig. 18. Comparison of average equivalent bubble radiuses with different mass flow rates

3. CONCLUSIONS

The processes of bubble growth in 1.8 mm-gap rectangular channel and 2.8 mm-gap rectangular channel have been visually and numerically studied. Two conclusions can be drawn from the work:

1. Bubbles behave differently in two channels for the bubble growth force will increase dramatically in micro channel. The size of bubbles in 1.8mm-gap channel is smaller than that in 2.8mm-gap channel under similar flow and heating conditions. Bubbles in 1.8mm-gap channel are more obviously affected by bubble growth force and will have small fluctuations in size during growth process, while the bubbles generated in 2.8mm-gap channel can lift off from the wall more easily, because the bubble growth force is not significant.
2. In the experimental range, the increase of heating power can affect the bubble growth but there is no obvious law. The increase of inlet fluid temperature can significantly increase the bubble growth rate and bubble size while the change of mass flow rate has little influence on bubble growth in both channels.

Acknowledgements

This study is supported by National Natural Science Foundation of China (Grant No. 11305169) and the National Key R&D Program of China (No.2017YFE 0300604).

Nomenclature

g	Gravitational constant (m/s^2)
D_h	Hydraulic diameter (m)
Co	Confinement number

a, b, c Bubble axises in three directions (m)
R The equivalent bubble radius (m)
k, n Empirical parameters
t Time (s)
M Mass flow rate (kg/h)
T_{in} Inlet fluid temperature (°C)
P Heating power (W)
T_a Average fluid temperature (°C)
L_n The distance from the nucleation point to the start point of heating section (m)
c_p Specific heat capacity of water (J/kg°C)
L_t Total length of heating section (m)
F_s Surface tension force (N)
F_{gr} Bubble growth force (N)
F_{sl} Shear lift force (N)
F_{cp} Contact pressure force (N)
F_r Reaction force caused by wall (N)
F_{bulk} Additional added-mass force (N)
F_{qs} Quasi steady drag force (N)
F_b Buoyancy force (N)
d_w Bubble contact circle diameter (m)
C_s, Empirical constant
C_{L1}, C_{L2} Empirical constant
A Bubble cross section area (m^2)
U_c Velocity (m/s)
V_b Bubble volume (m^3)
e_x Unit vector in X direction
r_c Radius of curve (m)
H Height of channel (m)

Greek Letters

ρ_l Density of liquid (kg/m^3)
ρ_v Density of vapour (kg/m^3)
η Heating efficiency
σ Surface tension coefficient (N/m)
θ_a Advancing contact angle (°)
θ_r Receding contact angle (°)
θ_c Bubble incline angle (°)
ω Vorticity
α Maximum local void fraction
β Bubble aspect ratio

References

[1] Kandlikar S.G. Two-Phase Flow Patterns, Pressure Drop and Heat Transfer During Boiling in Mini channel Flow Passages of Compact Heat Evaporators, *Heat Transfer Engineering*, 2002, 23(5): 5-23

[2] S. S. Mehendale, A.M. Jacobi, R.K. Shah, Fluid Flow and Heat Transfer at Micro- and Macro- Scales with Application to Heat Exchanger Design, *Appl. Mech. Rev*. 53 ,2000 175-193.

[3] P.A. Kew, K, Cornwell, Correlations for the Prediction of Boiling Heat Transfer in Small Diameter Channels, *Appl. Therm. Eng*. 17, 1997, 705-715.

[4] Azbel D. Two-Phase Flow in Chemical Engineering. Cambridge University Presentation, USA, 1981.

[5] Forster, H.K., Zuber, N. Growth of vapor bubbles in superheated liquid. *Journal of Applied Physics* 25, 1954, 474–478.

[6] Deqi Chen, Liangming Pan and Song Ren. Prediction of Bubble Detachment Diameter in Flow Boiling Based on Force Analysis. *Nuclear Engineering and Design.* 243, 2012, 263-271.

[7] Thorncroft, G.E., Klausner, J.F., Mei, R., 2001. Bubble Forces and Detachment Models. *Multiphase Science and Technology* 13, 35–76

[8] Klausner, J.F., Mei, R., Bernhatd, D.M., et al. Vapour Bubble Departure in Forced Convection Boiling. *International Journal of Heat and Mass Transfer* 1993, 36 (3), 651–662.

[9] Van Helden, W.G.J., Van der Geld, C.W.M., Boot, P.G.M. Forces on Bubbles Growing and Detaching in Flow along a Vertical Wall. *International Journal of Heat and Mass Transfer*. 1995, 38 (11), 2075–2088.

[10] Liaofei Yin, Li Jia. Confined Bubble Growth and Heat Transfer Characteristics during Flow Boiling in Micro-channel. *International Journal of Heat and Mass Transfer* 98 ,2016, 114–123

[11] Liaofei Yin, Li Jia. Confined Characteristics of Bubble during Boiling in Micro-channel. *Experimental Thermal and Fluid Science.*74, 2016, 247-256.